

Power-law scaling during shadowing growth of nanocolumns by oblique angle deposition

F. Tang^{a)}

Department of Physics, Applied Physics and Astronomy, Rensselaer Polytechnic Institute, 110 8th Street, Troy, New York 12180-3590

T. Karabacak

Department of Applied Science, University of Arkansas at Little Rock, Little Rock, Arkansas 72204

L. Li, M. Pelliccione, G.-C. Wang, and T.-M. Lu

Department of Physics, Applied Physics and Astronomy, Rensselaer Polytechnic Institute, 110 8th Street, Troy, New York 12180-3590

(Received 18 August 2006; accepted 14 November 2006; published 3 January 2007)

The authors have investigated the power-law behaviors of various morphological parameters during the shadowing growth of ruthenium (Ru) nanocolumns by an oblique angle sputter deposition technique with substrate rotation. Particularly, wavelength and column number density were measured at different column heights (h). The exponents associated with the wavelength (p_λ) and column number density (p_n), correlated by the geometrical relationship $p_\lambda \approx -\frac{1}{2}p_n$, were measured by atomic force microscopy to be ~ 0.5 and ~ -1.0 , respectively. Using a one-dimensional facet growth model based upon the principle of evolutionary selection under oblique angle deposition, they showed that the exponents associated with the column number density and wavelength can be predicted. The authors also illustrated that the exponent value associated with column number density originates from the competitive growth among columns that have different vertical growth rates. The simulated exponent values are independent of the shape of the facet, which indicates the universality of these power-law exponents. © 2007 American Vacuum Society.

[DOI: 10.1116/1.2406059]

I. INTRODUCTION

Surface morphology is known to control many physical properties of thin films. Different deposition techniques can produce various surface morphologies of thin films. An interesting development in the control of film morphology is the use of oblique angle physical vapor deposition with substrate rotation.¹⁻⁷ Many fascinating new nanostructures can be formed. An example is the formation of physical self-assembled vertical nanocolumns through the shadowing effect.^{8,9} The shadowing effect originates from a non-normal incident flux where the obliquely incident particles cannot reach the lower lying surface points because they are “shadowed” by taller surface features in the neighbors.

Many quantitative studies of morphology parameters of nanostructures, mainly the quasiperiodic wavelength and column width, were recently reported. Based on a dynamic scaling theory and the results of Monte Carlo simulations, Karabacak *et al.*⁸ predicted that the column width during oblique angle deposition with substrate rotation would grow as a power-law form $W \sim h^{p_w}$ with the exponent $p_w \approx 0.3$ when surface diffusion is high and $p_w \approx 0.5$ when surface diffusion is neglected. In the same study they showed experimentally by the cross sectional scanning electron microscopy (SEM) images that $p_w \approx 0.28-0.34$ for the growth of Cu, Co, W, and Si nanocolumns under large oblique incident angle by measuring survived long rods. Recently, Buzea *et al.*¹⁰ measured

column width exponent to range from 0.3 to 0.6 for amorphous silicon (*a*-Si) nanocolumns deposited at various obliquely incident angles between 75° and 89°. Moreover, based on the *a*-Si structure Kaminska *et al.* obtained $p_w = 0.50 \pm 0.09$.¹¹ In contrast to the column width exponent, the wavelength exponent p_λ is shown to be ~ 0.5 regardless of the deposition materials. For example, Kaminska *et al.* obtained $p_\lambda = 0.55 \pm 0.07$ for *a*-Si rods.¹¹ Karabacak *et al.* previously also reported the existence of wavelength selection in tungsten (W) nanocolumns using an oblique angle sputter deposition technique.¹² However, in that work, the change of the peak position in the power spectral density (PSD) is empirically fitted according to an exponential decay function. A reanalysis of the experimental data using a power-law fit gives $p_\lambda = 0.58 \pm 0.05$. Although the exponent of the wavelength indicates a universality, which is not sensitive to the deposition materials, there is still no in-depth understanding in the physical origin of this wavelength evolution in shadowing growth.

In this article we first investigated growth exponents associated with the wavelength and the column number density of Ru nanocolumns. The growth exponent of the wavelength can be geometrically correlated to the growth exponent of column number density, which is a statistical measure of survived columns under shadowing growth in contrast to the column width⁸ that strongly depends on noise and surface diffusion. To understand the scaling behaviors, we investigated a facet growth model, which is based upon the principle of evolutionary selection proposed by van der Drift¹³

^{a)}Electronic mail: tangf2@rpi.edu

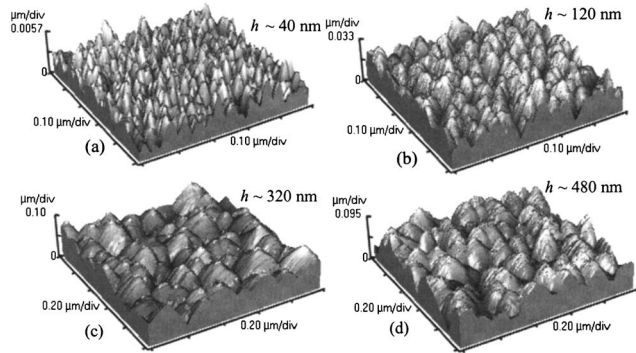


FIG. 1. Atomic force microscopy images of Ru nanocolumns of various average heights h (a) ≈ 40 nm, (b) ≈ 120 nm, (c) ≈ 320 nm, and (d) ≈ 480 nm. The scan size of images (a) and (b) is $0.5 \times 0.5 \mu\text{m}^2$. For images (c) and (d) the scan size is $1 \times 1 \mu\text{m}^2$. The vertical scale varies from image to image. The labeled thickness h was measured from the SEM cross sectional images of Ru nanocolumns.

and Paritosh and Srolovitz.¹⁴ Using simulations we showed that the exponents associated with the column number density and wavelength can be predicted using the facet growth model. Combining the experimental measurements and modeling, the geometrical origin of the power-law evolutions of column number density was illustrated. This geometrical origin also provides physical insight into the evolution of wavelength, which is inherently related to the evolution of column number density. The present findings are complementary to the existing theories^{8,15} on the dynamic evolution process during oblique angle deposition.

II. EXPERIMENT

A dc magnetron sputtering system was used to deposit Ru nanocolumns on a Si(100) surface with native oxide. Details of the experimental setup have been described elsewhere.⁹ During the deposition, the substrate normal had an angle of 85° with respect to the target surface normal and the substrate was rotating around its surface normal with a speed of 30 rpm. The deposition rate of the oblique angle depositions of Ru nanocolumns was measured to be approximately 4 nm/min from cross-sectional SEM images. The quantitative surface morphology was measured using noncontact mode atomic force microscopy (AFM) with a scan size of 512×512 pixels. The radius of the silicon tip was about 10 nm, and the side angle was approximately 12° .

III. EXPERIMENTAL RESULTS AND ANALYSIS

AFM images were taken on a series of deposited films, typically shown in Figs. 1(a)–1(d). The columns that are shadowed by neighboring taller columns stop growing, which leads to an increased average column-column separation (i.e., center-to-center separation of the columns). The scan sizes of the images are $0.5 \times 0.5 \mu\text{m}^2$ for $h < 300$ nm and $1 \times 1 \mu\text{m}^2$, for thicker samples. The thickness h labeled in the AFM images in Fig. 1 was measured from the SEM cross sectional images of Ru nanocolumns.⁹

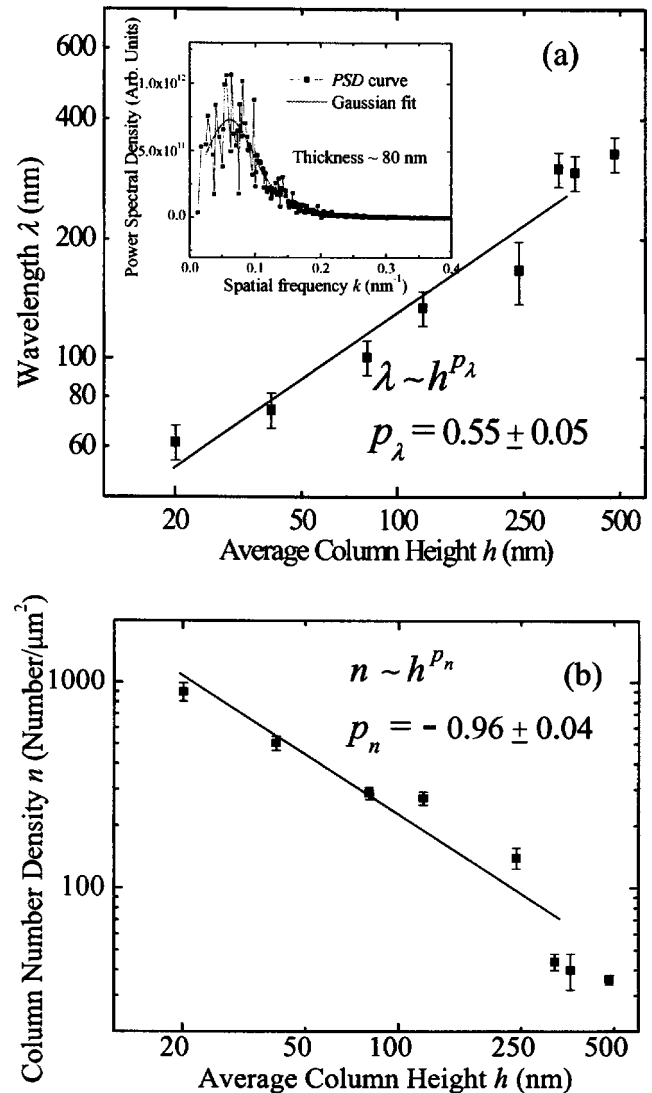


FIG. 2. Plots of (a) wavelength and (b) column number density as a function of average column height h in log-log scale and the corresponding linear fits. The values in the parentheses correspond to exponents extracted from the linear fits. The linear fits applied to data with $h < 350$ nm. The inset in the top left of (a) shows an example of the PSD curve of the Ru nanorods with 20 min (~ 80 nm) deposition and its Gaussian fit around the peak of the PSD curve.

A. Wavelength selection (column-column separation)

It has been shown previously that for tungsten nanocolumns,¹² the column-column separation can have a characteristic length λ (“wavelength”) and can give a quasi-periodic nanocolumn morphology. “Wavelength selection” reflects the time evolution of λ , and in our study of Ru nanocolumns it will be extracted from the Fourier space analysis of the AFM images. A quasi-periodic morphology is reflected as a peak in the two-dimensional (2D) PSD plot. For an isotropic surface, the PSD is a function of the spatial frequency k .¹² The inset in the top left of Fig. 2(a) shows an example of a PSD curve of the Ru nanocolumns with 20 min (~ 80 nm) deposition. The position of the peak at a spatial frequency k_{max} corresponds to a wavelength λ through the relation $\lambda = 2\pi/k_{\text{max}}$. The k_{max} is obtained by a Gaussian fit

around the peak of the PSD curve, which is used to calculate the wavelength through the relation $\lambda = 2\pi/k_{\max}$. Figure 2(a) shows the values for λ measured at various average column heights h and plotted in log-log scale. The error bar of the wavelength is the standard deviation of the wavelengths obtained from different AFM images measured from the same sample. A linear fit to the experimental data reveals that the wavelength changes with column height according to a power-law behavior $\lambda \sim h^{p_\lambda}$, where the “wavelength exponent” value is extracted to be $p_\lambda = 0.55 \pm 0.05$. We note that the linear fit in Fig. 2(a) was performed over heights of less than approximately 350 nm. The columnar growth starts to saturate after the height reaches about 350 nm, where the lateral size and number of columns do not change significantly, but their heights continue to increase.

B. Column number density

We define the “column number density” n as the number of nanocolumns per given substrate area. The column number density along with the maximum column height can quantitatively reflect the competition among columns during growth. For the measurement of column number density n , we used a software package (Scanning Probe Image Processor Version 3.3.5.0) to analyze the Ru AFM images at different average column heights h . The column number density n was extracted using a grain analysis method (with the watershed model and gradient norm). Figure 2(b) plots the change of n (in units of number/ μm^2) with the average column height h in log-log scale. It is realized that the number density does not change significantly after the height values reach about 350 nm, where the saturation in the growth begins. The linear fit before the saturation in Fig. 2(b) reveals the power-law functional behavior $n \sim h^{p_n}$, where the measured number density exponent $p_n = -0.96 \pm 0.04$.

The exponent p_λ can be correlated to p_n by using the relationship between the column number density and the wavelength. For a 2D quasiperiodic array of nanocolumns separated by an average wavelength λ , it has a geometrical relationship of $\lambda^2 \sim 1/n$. The substitution of the power-law forms $\lambda \sim h^{p_\lambda}$ and $n \sim h^{p_n}$ to this relationship gives $p_\lambda \approx -\frac{1}{2}p_n$. Therefore, the measured value of $p_n \approx -0.96$ described above leads to the predicted value $p_\lambda \approx 0.48$, which is close to our experimental result, $p_\lambda = 0.55$. These two exponents are independent of the exponent associated with the growth of column width that strongly depends on noise and surface diffusion.⁸

IV. DISCUSSION

The number density of surviving columns has been studied by Meakin and Krug¹⁶ and Krug,¹⁷ using a 1+1 dimension needle model. This model corresponds to the simplest and extreme case of shadowing where shadowed needles receive no incident flux, representative of oblique angle deposition. The shadowing growth is noise driven by the random deposition among the survived needles. By projecting the heights of surviving needles to an axis perpendicular to the substrate, the shadowing growth becomes a process of coa-

lescing random walk. It was found that $n \sim h^{-1/2}$, where h is the height of the surviving needles. The exponent of n needs to be doubled when considering the extra lateral dimension in the 2+1 dimensions, which is then equal to -1.0 . This predicted value is remarkably close to our experimental value despite the unrealistic nature of the needles. A natural way to include the morphology information is to replace every needle with a crystal having a finite lateral dimension or rodlike, which produces a similar model used by Paritosh and Srolovitz.¹⁴ We now consider this rodlike model to correlate the geometrical effect during the growth under shadowing.

A. Facet growth model: Simulations

In the work by Paritosh and Srolovitz,¹⁴ the evolution of the crystal orientation under oblique angle deposition with a fixed substrate was investigated using a 1+1 model. The effect of noise is included in the initial random distribution of crystal orientation. The model is based on the growth of an array of facet crystals. Each facet grows normal to itself at a speed of $-\mathbf{J} \cdot \hat{n}$, which is proposed by van der Drift.¹³ \mathbf{J} is the flux and \hat{n} is the unit vector perpendicular to the facet. see Fig. 3. Here we modify this model to consider the substrate rotation. Based on this modified model, we will give a detailed analysis of the scaling phenomenon. Figure 3 shows a schematic of the modified facet growth model. To mimic the substrate rotation, we divided the growth process into two steps in which the flux comes from the right (\mathbf{J}_R) and left sides (\mathbf{J}_L) alternatively, see Figs. 3(a) and 3(b), respectively. The values of \mathbf{J}_R and \mathbf{J}_L are same, represented by J . The α is the vapor incident angle measured with respect to the substrate normal. The angle between the two top facets of the crystals is kept fixed in the simulation. However, the crystals can be tilted or vertically oriented, which are labeled by C and D , respectively. The tilt angle β' of the crystal is measured between the bisector line of the angle γ between the two top facets and the substrate normal. The simulation tracks the movements of vertices, such as A and B shown in Fig. 3(a), the intersections between facets. The position of a new vertex will be determined by the flux received by the two neighboring facets that form the vertex. For example, the left facet L and A is shadowed; therefore the new position of vertex A' will have a perpendicular distance $-\mathbf{J}_R \cdot \hat{n}$ to the right facet R and a zero distance to facet L . If the new vertex was shadowed after one step of deposition according to this growth rule, it would move slightly along the new facet R' to a new point B' not being shadowed. New vertices will be added at places on the facets where the shadowed part and nonshadowed part meet or at the intersection of two crystal planes.

In this model the receiving flux would not redistribute itself among the facets. Therefore the model would be suitable to describe the evolution process under a low surface diffusion case and the result is determined by shadowing effects and geometrical factors. At the beginning of the growth, a number of small crystals with various tilted angle are assumed to nucleate on the substrate simultaneously. This

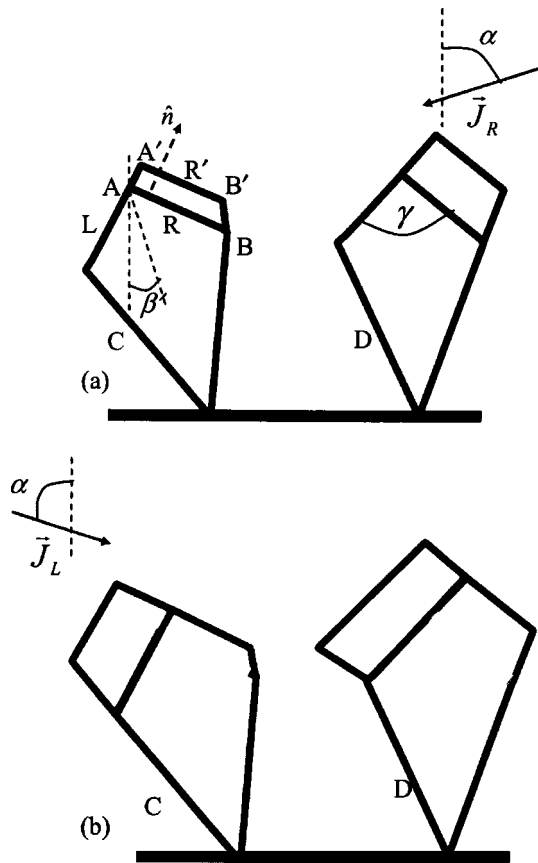


FIG. 3. Schematic of facet growth model. (a) The flux \mathbf{J}_R comes from the right. The α is the vapor incident angle measured from the substrate normal. Each facet grows normal to itself at a speed of $-\mathbf{J}_R \cdot \hat{n}$, where \hat{n} is the unit vector perpendicular to the facet. Point A is the intersection between facet L and facet R . In one step of growth the vertex $A(B)$ moves to $A'(B')$. The R' is the newly formed facet. The γ is the angle between two top facets. The β^* is the tilting angle of the nanocolumn, measured from the bisector line of the angle γ between two facets and substrate normal. (b) The flux \mathbf{J}_L comes from the left.

assumption is consistent with the observed random crystal-line orientation detected by reflection high energy electron diffraction.⁹ The initial dispersion of the crystals' tilted angles has a broad Gaussian distribution. The initial spaces between nuclei are set to be random. To investigate the effect of the different geometry of crystals the angle between top facets γ is chosen as 60° or 120° . In order to obtain good statistical results, 1000 nuclei were chosen in each simulation. The data reported below were averaged over at least four independent simulations.

In Fig. 4(a), a side view of simulated growth with flux incident angles $\alpha=85^\circ$ and $\gamma=60^\circ$ is shown (only a limited range in the horizontal axis is displayed). We can see that with more deposition only those columns having smaller tilt angles will survive due to their higher vertical growth rate. Figures 4(b) and 4(c) show the quantitative results of the dynamic behaviors extracted from the simulated data for different γ values (60° or 120°). To obtain the number of surviving columns, we make a cut (from the side view of the columnar structure) at certain heights and count those that have the intersections with the cut. The wavelength is deter-

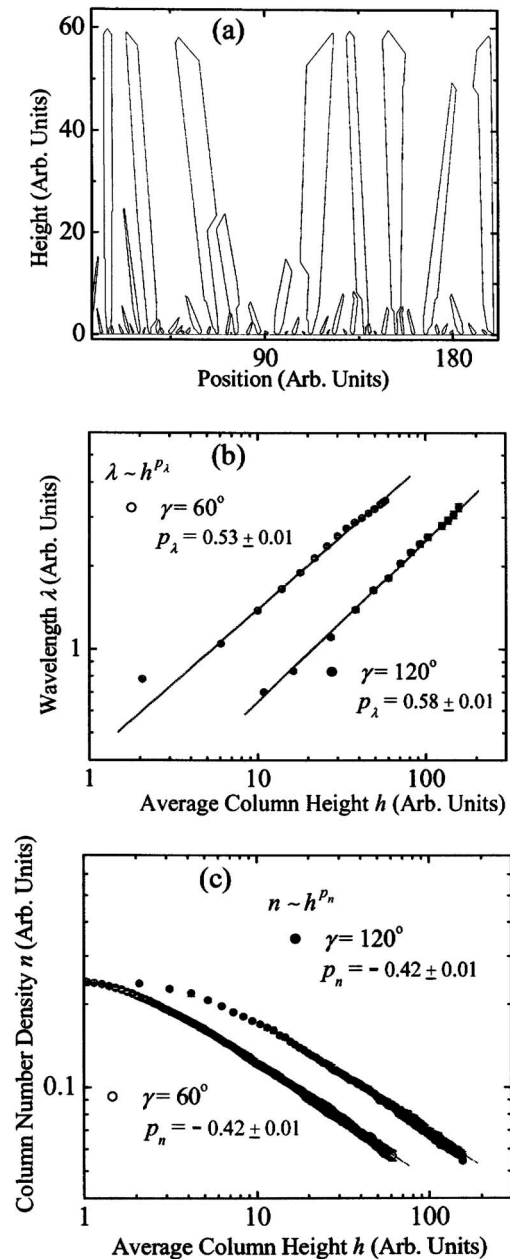


FIG. 4. Side view of simulated growth using the facet growth model for vapor fluxes incident at 85° . The plots of (b) wavelength and (c) column number density as a function of average column height in log-log scale and the corresponding linear fits. The values in the parentheses are corresponding exponents from the linear fits.

mined by the peak in the one-dimensional PSD plot. From Fig. 4(b), we can see that although the absolute value of wavelength depends on the facet angle γ , the exponent associated with it is almost same. The value of p_λ is 0.53 ± 0.01 ($\gamma=60^\circ$) or 0.58 ± 0.01 ($\gamma=120^\circ$), which is consistent with the experimental result (0.55 ± 0.05).

In Fig. 4(c), the exponent associated with the column number density is shown to be -0.42 ± 0.01 by the linear fit for long deposition times. In the very beginning stage the column number density has a slower decreasing rate, which does not fit the power law. This is due to the fact that there is

no shadowing effect when the crystals are initially nucleated. Therefore, there will be a transition stage to the dominance of shadowing effect where the power law starts to appear. Real films are isotropic (in the substrate plane) and they represent 2+1 dimensional case while the 1+1 model only represents a cross section of the three-dimensional space. Therefore, the exponent of the column number density (n) needs to be doubled for real films, which becomes -0.84 ± 0.02 . This value is compared with the experimental result of -0.96 ± 0.04 . Considering the simplicity of the model the result is reasonable.

B. Facet growth model: An analytical approach

A geometrical argument can also be made to provide physical insight of the facet growth model. Here we will just investigate the evolution of column number density. Under the shadowing growth, the taller columns will survive, therefore the crystal having the highest vertical growth rate will determine the growth. It will be very important to know the vertical growth rate in order to gain an in-depth understanding. Figure 5(a) shows a schematic of the growth of a single crystal column. The tilt angle of the crystal column is β' . After one deposition including the flux coming from the left and right, the vertex moves from initial A to A' . The growth

vector $\mathbf{V}(\beta')$ which is a function of the tilt angle β' can be divided into two components $\mathbf{V}_R(\beta')$ and $\mathbf{V}_L(\beta')$ which are parallel to the facets L and R , respectively,

$$\mathbf{V}(\beta') = \mathbf{V}_R(\beta') + \mathbf{V}_L(\beta'). \quad (1)$$

$\mathbf{V}_{nR}(\beta')$ and $\mathbf{V}_{nL}(\beta')$ are the growth rates perpendicular to the facets due to the flux coming from the right and left, respectively. Their values are

$$\begin{aligned} V_{nR}(\beta') &= J \sin(\alpha + \beta' + \gamma/2), \\ V_{nL}(\beta') &= J \sin(\alpha - \beta' + \gamma/2). \end{aligned} \quad (2)$$

The angle between $\mathbf{V}_R(\beta')$ and $\mathbf{V}_{nR}(\beta')$ or $\mathbf{V}_L(\beta')$ and $\mathbf{V}_{nL}(\beta')$ is $90^\circ - \gamma$, so

$$\begin{aligned} V_R(\beta') &= \frac{J \sin(\alpha + \beta' + \gamma/2)}{\sin(\gamma)}, \\ V_L(\beta') &= \frac{J \sin(\alpha - \beta' + \gamma/2)}{\sin(\gamma)}. \end{aligned} \quad (3)$$

The angle between $\mathbf{V}_R(\beta')$ and the substrate normal is $\gamma/2 - \beta'$ and the angle between $\mathbf{V}_L(\beta')$ and the substrate normal is $\gamma/2 + \beta'$. Considering Eq. (1) then the vertical $\mathbf{V}_\perp(\beta')$ and parallel components $\mathbf{V}_\parallel(\beta')$ of $\mathbf{V}(\beta')$ are, respectively,

$$\begin{aligned} V_\perp(\beta') &= J \frac{\sin(\alpha + \beta' + \gamma/2)\cos(\gamma/2 - \beta') + \sin(\alpha - \beta' + \gamma/2)\cos(\gamma/2 + \beta')}{\sin(\gamma)}, \\ V_\parallel(\beta') &= J \frac{\sin(\alpha + \beta' + \gamma/2)\sin(\gamma/2 - \beta') - \sin(\alpha - \beta' + \gamma/2)\sin(\gamma/2 + \beta')}{\sin(\gamma)}. \end{aligned} \quad (4)$$

After a simplification, these equations become

$$\begin{aligned} V_\perp(\beta') &= J \frac{\sin(\alpha + \gamma) + \sin \alpha \cos(2\beta')}{\sin(\gamma)}, \\ V_\parallel(\beta') &= J \frac{-\sin(\alpha)\sin(2\beta')}{\sin(\gamma)}. \end{aligned} \quad (5)$$

For a small tilt angle β' , it can be further simplified into

$$\begin{aligned} V_\perp(\beta') &= J \left(\frac{\sin(\alpha + \gamma) + \sin \alpha}{\sin(\gamma)} \right) - J \left(\frac{2 \sin \alpha}{\sin(\gamma)} \right) \beta'^2, \\ V_\parallel(\beta') &= -2J \frac{\sin(\alpha)}{\sin(\gamma)} \beta'. \end{aligned} \quad (6)$$

The top vertex of the column will move at a constant speed given by Eq. (6). This is consistent with our observed constant experimental deposition rate. When the highest vertex is shadowed, the entire column will also be shadowed and ceases to grow. Furthermore, the top vertices of the non-

growing columns are shadowed by the top vertices of nearby columns, which are the highest points in their individual columns. Therefore, for tracking the survived columns, we just need to consider the movements of top vertices. The vertical columns have the highest vertical growth rate. So below we consider the geometry where the tilted column is shadowed by the nearby vertical column. In Fig. 5(b), the traces of the top vertex of a tilted and vertical column are represented by needles C and D . From the above arguments, the competition between the two columns can be reduced to the competition between the two needles. This model has been applied by Tang *et al.* to study the scaling behavior in Ru texture evolution.⁹ We take the case that the needle C is shadowed from the right by the needle D as an example. At the initial stage the tilted needle C will not be shadowed by the vertical needle D , due to a very small height difference between them. As the deposition continues, the vertical height difference Δh will increase and the tilted needle C will finally be shadowed by D . From Eq. (6), under a small angle of β' , the

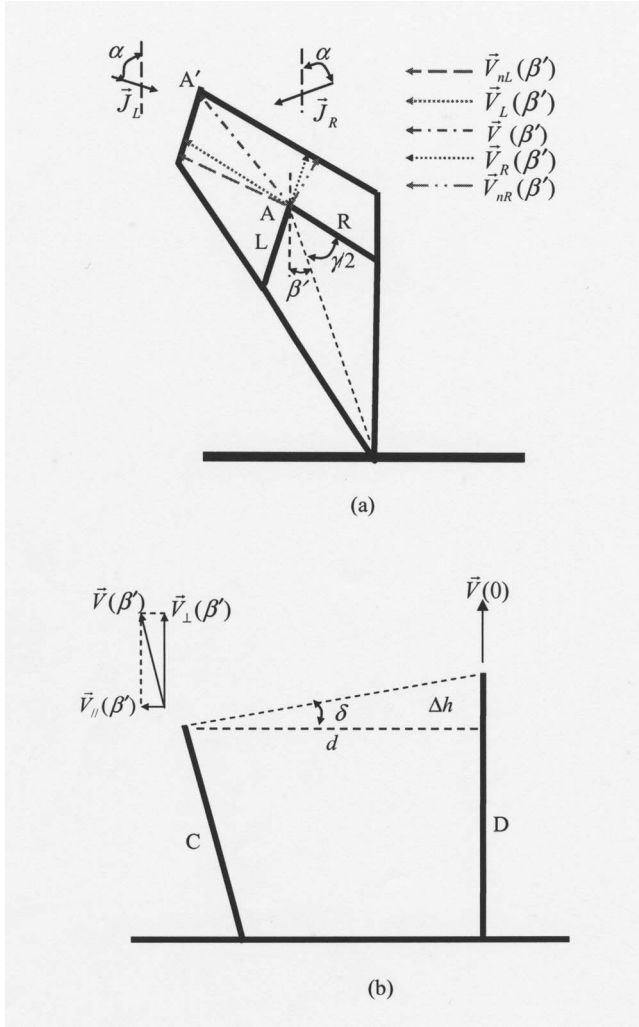


Fig. 5. (a) Schematic of the growth of one column after one deposition including fluxes coming from the right and left. The β' is the tilting angle of a column, measured between the bisector line of the angle between two facets and substrate normal. The γ is the angle between two facets. The \mathbf{J}_L and \mathbf{J}_R are the vapor flux coming from the left and right, respectively. The growth vector $\mathbf{V}(\beta')$ can be divided into two components $\mathbf{V}_R(\beta')$ and $\mathbf{V}_L(\beta')$ which are parallel to the R and L facets, respectively. The $\mathbf{V}_{nR}(\beta')$ and $\mathbf{V}_{nL}(\beta')$ are growth rates perpendicular to the facets due to the flux coming from the right and left, respectively. The velocity and its components are represented by different styles of dashed lines and colored arrows. (b) A schematic showing the competition between needles for studying column density evolution. The needle $C(D)$ represents the trace of the vertex of the tilted (vertical) rod along its speed direction $\mathbf{V}(\beta')$ ($\mathbf{V}(0)$). The $\mathbf{V}_\perp(\beta')$ and $\mathbf{V}_\parallel(\beta')$ are vertical and parallel components of $\mathbf{V}(\beta')$. The δ is the angle between the line going through the top ends of the needles C and D and the horizontal line. The Δh and d are the developed vertical height difference and lateral distance between the two needles, respectively.

vertical growth rate difference between the vertical and slanted needles is $\sim \beta'^2$. Therefore, after a growth time t , Δh will be

$$\Delta h \sim t\beta'^2. \quad (7)$$

The survived needles without being shadowed from the right are those satisfying the nonshadowing condition, which is given by

$$\tan(\delta) = \frac{\Delta h}{d} < \frac{\pi}{2} - \alpha, \quad (8)$$

where δ is the angle between the line going through the top ends of needles C and D and the horizontal line, and d is the shortest distance between the top of needle C to needle D . The lateral growth rate of the tilted column is $\sim \sin(\beta')$. Since we are interested in the small angle approximation of β' , this lateral growth rate will be $\sim \beta'$, which is much smaller than the vertical growth rate of the tilted column ($\sim 1 - \beta'^2/2$). Therefore we ignore the change of d during the growth. Once the needle is shadowed from the right, it will receive much less flux that leads to rapidly decreasing of the growth rate. Due to the much slower growth rate of the needle, it will be fully shadowed quickly. Therefore combining Eqs. (7) and (8), the maximum of the allowed tilting angle of survived needles should satisfy the condition

$$\beta'_{\max}(t) \sim t^{-0.5}. \quad (9)$$

If we assume that the distribution of α has a Gaussian distribution, then the number of survived rods will be $n \sim \beta'_{\max}(t)n_0$. The n_0 is the column number with a vertical orientation. During the growth, vertical columns will never be shadowed due to its highest vertical growth rate. Therefore n_0 will be constant during the growth. This leads to $n \sim \beta'_{\max}(t) \sim t^{-0.5}$, where the exponent value of number density is evaluated to be -0.5 (for the $2+1$ dimension, the exponent becomes -1). Remarkably, this value is identical to that obtained by the $1+1$ needle model derived by Main *et al.*¹⁵ and Meakin and Krug¹⁶ using a random walk argument. From the above analysis, we can see that the exponent value is not related to the shape of a crystal determined by the angle of γ , which is consistent with our simulation results. The shape of the column may be different for different materials. However, through the above analysis we can argue that the exponent of the column density is universal and is independent of materials.

V. CONCLUSION

In conclusion, we have presented a detailed study of morphological evolution of Ru nanocolumns during oblique angle deposition with substrate rotation. It was observed that the nanocolumns generated a quasiperiodic surface topography as a result of the shadowing effect. The exponents for the evolution of wavelength and column number density are measured as $p_\lambda \sim 0.5$ and $p_n \sim -1.0$, respectively. Based on geometrical arguments, p_n is correlated to p_λ by $p_n \approx -2p_\lambda$. Moreover, simulations of a facet growth model of oblique angle deposition mimicking substrate rotation also revealed the power-law evolution of the surface parameters having exponent values consistent with the experimental results and showed the universality of p_n .

ACKNOWLEDGMENTS

The work was supported by the NSF-NIRT (ECS-0506738). One of the authors (M.P.) was supported by the NSF Research Experience for Undergraduates (REU) (PHY-

0453231) and Undergraduate Research Program (URP) at Rensselaer. Another author (F.T.) was supported by Meiners Fellowship. The authors thank D.-X. Ye for taking the scanning electron microscopy images of the samples.

¹K. Robbie and M. J. Brett, *J. Vac. Sci. Technol. A* **15**, 1460 (1997).

²Y.-P. Zhao, D.-X. Ye, G.-C. Wang, and T.-M. Lu, *Nano Lett.* **2**, 351 (2001).

³K. Robbie, M. J. Brett, and A. Lakhtakia, *Nature (London)* **384**, 616 (1996).

⁴H. Alouach and G. J. Mankey, *J. Vac. Sci. Technol. A* **22**, 1379 (2004).

⁵M. O. Jensen and M. J. Brett, *IEEE Trans. Nanotechnol.* **4**, 269 (2005).

⁶M. O. Jensen and M. J. Brett, *Proc. SPIE* **5380**, 91 (2005).

⁷A. Lakhtakia and R. Messier, *Sculptured Thin Films: Nanoengineered*

Morphology and Optics (SPIE, 2005), Chap. 1, p. 7.

⁸T. Karabacak, J. P. Singh, Y.-P. Zhao, G.-C. Wang, and T.-M. Lu, *Phys. Rev. B* **68**, 125408 (2003).

⁹F. Tang, T. Karabacak, P. Morrow, C. Gaire, G.-C. Wang, and T.-M. Lu, *Phys. Rev. B* **72**, 165402 (2005).

¹⁰C. Buzea, G. Beydaghyan, C. Elliott, and K. Robbie, *Nanotechnology* **16**, 1986 (2005).

¹¹K. Kaminska, A. Amassian, L. Martinu, and K. Robbie, *J. Appl. Phys.* **97**, 013511 (2005).

¹²T. Karabacak, G.-C. Wang, and T.-M. Lu, *J. Appl. Phys.* **94**, 7723 (2003).

¹³A. van der Drift, *Philips Res. Rep.* **22**, 267 (1967).

¹⁴F. Paritosh and D. J. Srolovitz, *J. Appl. Phys.* **91**, 1963 (2002).

¹⁵E. Main, T. Karabacak, and T.-M. Lu, *J. Appl. Phys.* **95**, 4346 (2004).

¹⁶P. Meakin and J. Krug, *Phys. Rev. A* **46**, 3390 (1992).

¹⁷J. Krug, *Adv. Phys.* **46**, 139 (1997).